

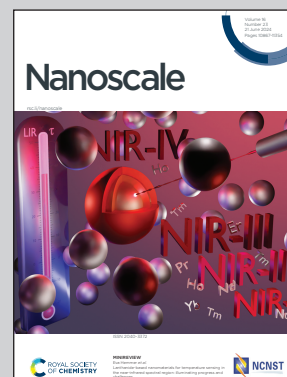


Showcasing research from the Personick Research Group, Department of Chemistry, University of Virginia, Charlottesville, Virginia, USA.

Troubleshooting the influence of trace chemical impurities on nanoparticle growth kinetics *via* electrochemical measurements

Just as sheet music represents a benchmark for reproducing a musical performance, work by Halford, McDarby, *et al.* demonstrates that open-circuit potential measurements of colloidal nanoparticle syntheses provide a way of benchmarking the real-time chemistry of nanoparticle growth. This information can then be used to streamline troubleshooting of irreproducibility in nanoparticle synthesis and to directly translate colloidal syntheses methods to electrodeposition-based nanoparticle growth.




As featured in:



See Michelle L. Personick *et al.*, *Nanoscale*, 2024, **16**, 11038.


 Cite this: *Nanoscale*, 2024, **16**, 11038

## Troubleshooting the influence of trace chemical impurities on nanoparticle growth kinetics *via* electrochemical measurements†

 Gabriel C. Halford,  ‡<sup>a,b</sup> Sean P. McDarby,  ‡<sup>b</sup> Sebastian Hertle,  <sup>a,b</sup>  
 Anne F. Kiely,<sup>b</sup> Jessica T. Luu,<sup>b</sup> Claire J. Wang<sup>b</sup> and Michelle L. Personick  \*<sup>a,b</sup>

Reproducibility issues resulting from particle growth solutions made with cetyltrimethylammonium bromide (CTAB) surfactant from different lots and product lines in a newly developed synthesis of mono-metallic palladium (Pd) tetrahedra (THH) nanoparticles are investigated *via* a multi-pronged approach. Time-resolved electrochemical measurements of solution potential, variation of chemical parameters in colloidal synthesis, and correlation to electrodeposition syntheses are used together to uncover the effects of the unknown contaminants on the chemical reducing environment during nanoparticle growth. Iodide—a known impurity in commercial CTAB—is identified as one of the required components for equalizing the reducing environment across multiple CTAB sources. However, an additional component—acetone—is critical to establishing the growth kinetics necessary to enable the reproducible synthesis of THH in each of the CTAB formulations. In one CTAB variety, the powdered surfactant contains too much acetone, and drying of the as-received surfactant and re-addition of solvent is necessary for successful Pd THH synthesis. The relevance of solvent impurities to the reducing environment in aqueous nanoparticle synthesis is confirmed *via* electrochemical measurement approaches and solvent addition experiments. This work highlights the utility of real-time electrochemical potential measurements as a tool for benchmarking of nanoparticle syntheses and troubleshooting of reproducibility issues. The results additionally emphasize the importance of considering organic solvent impurities in powdered commercial reagents as a possible shape-determining factor during shaped nanomaterials synthesis.

Received 5th January 2024,

Accepted 24th April 2024

DOI: 10.1039/d4nr00070f

[rsc.li/nanoscale](https://rsc.li/nanoscale)

## Introduction

The reliable and reproducible production of complex and high-quality shaped metal nanoparticles *via* protocols that involve precise tuning of chemical reaction environments during synthesis requires chemical sources that are either free of contaminants or have consistent known amounts of contaminants. An examination of the literature in the field of shaped nanoparticle synthesis reveals requirements for reagents from specific chemical suppliers, product lines, and/or lot numbers.<sup>1–8</sup> The major effects that small impurities can have on nanoparticle growth represent both a challenge and an opportunity for materials synthesis. Given the interest in using shaped nanoparticles for specialized and industrial

applications, including as selective catalysts, reproducibility issues in synthesis can be a substantial barrier to fundamental scientific advances.<sup>9</sup> However, if the subtleties of the chemical mechanisms underlying nanoparticle growth dynamics can be understood, they can be applied to the precise design of new materials.<sup>4–8,10</sup> Fully understanding the influence of even the smallest concentrations of contaminants is therefore paramount for streamlining industrial implementation, as well as saving significant cost from failed production attempts, and enabling the synthesis of presently unachievable nanoparticle morphologies.<sup>3–5,11,12</sup> Studying the influence of contaminants, however, can be difficult, due to the differences in methodologies needed to identify various kinds of elemental and molecular contaminants, ranging from nuclear magnetic resonance spectroscopy (NMR) to mass spectrometry (MS) to ion chromatography (IC) to inductively coupled plasma (ICP) spectroscopies. Further complexity is added by the interdependent nature of chemical variables in a nanoparticle growth solution. Additionally, many analytical approaches for studying the mechanisms of action of possible contaminants are time-consuming and/or costly, rendering their routine use somewhat prohibitive.

<sup>a</sup>Department of Chemistry, University of Virginia, Charlottesville, Virginia 22904, USA. E-mail: [mpersonick@virginia.edu](mailto:mpersonick@virginia.edu)

<sup>b</sup>Department of Chemistry, Wesleyan University, Middletown, Connecticut 06459, USA

† Electronic supplementary information (ESI) available. See DOI: <https://doi.org/10.1039/d4nr00070f>

‡ These authors contributed equally.



In this work, we report an aqueous colloidal synthesis for monodisperse, monometallic palladium (Pd) tetrahedra (THH). While examples of syntheses of colloidal Pd THH produced with the aid of a secondary metal, such as silver, can be found in the literature, and THH are a commonly observed high-index structure for other metals, few reports exist of monometallic Pd THH.<sup>13–16</sup> To our knowledge, monometallic Pd THH have previously only been produced electrochemically on an electrode surface using a square-wave potential and reported once colloiddally as part of a supersaturation-based shape control approach.<sup>17,18</sup>

Importantly, we determined that the success of this synthesis requires careful control of reaction kinetics, while subtle changes to the growth solution composition yield alternate shapes, such as concave cubes (CC) and terraced cubes (TC). We examine the critical role of the surfactant source in establishing the correct kinetic environment for the successful growth of Pd THH and provide a method for benchmarking synthesis conditions. The surfactant in every case is cetyltrimethylammonium bromide (CTAB), but changing between two high purity product lines from the same company (MilliporeSigma, formerly Sigma-Aldrich BioUltra (99.0%) and BioXtra (99%, Lot No. SLCJ8356)) or changing lot numbers within the same product line (BioUltra A, Lot No. BCCC5274 and BioUltra B, Lot No. BCCF7530) causes the synthesis to produce CC instead of THH. Extensive analysis was carried out to identify possible elemental and molecular contaminants present in each surfactant, and to understand the ways in which identified contaminants give rise to differences in nanoparticle growth kinetics that cause the discrepancies in product formation.

In particular, we demonstrate how our previously-reported approaches for electrochemical nanoparticle synthesis and time-resolved solution potential measurements<sup>19</sup> can be

applied to the troubleshooting of synthetic problems related to reagent contamination in nanoparticle synthesis. By understanding the reducing environment in which Pd particles are synthesized, our electrochemical toolkit can provide *in situ* information about the dynamic nature of the chemical environment during nanoparticle growth. Through comparison between *in situ* open-circuit potential measurements of successful and unsuccessful colloidal THH synthesis attempts alongside galvanostatic synthesis and chronopotentiometric measurement of the growth of shaped Pd particles adsorbed on an electrode surface, we can find a route toward resolving complicated synthetic roadblocks and pinpointing their origins. Specifically, in this case we identify the relevance of organic solvent impurities in powdered surfactants and their influence on particle syntheses and, with this information, we are then able to mitigate these contaminant effects and enable the reliable formation of monometallic Pd THH using multiple CTAB sources.

## Results and discussion

### Pd THH synthesis development

The Pd THH particle synthesis reported here uses a seed-mediated approach to colloidal growth. Large Pd nanocube seeds (~20 nm) were synthesized following a previously published method in which a hot solution of H<sub>2</sub>PdCl<sub>4</sub> in CTAB is reduced by ascorbic acid (AA).<sup>13</sup> These seeds were then diluted ten-fold and injected into an aqueous growth solution containing a Pd precursor (0.24 mM Na<sub>2</sub>PdCl<sub>4</sub>), nitric acid to control solution pH (0.61 to 1.21 mM HNO<sub>3</sub>), surfactant (50 mM CTAB), and additional AA (0.96 mM) as a reducing agent. The growth solution was allowed to react in a 40 °C water bath overnight. These conditions, particularly the use of 0.24 mM Pd precursor, will be referred to as “standard” reaction conditions throughout this work. Detailed experimental procedures can be found in the ESI.† With BioUltra A CTAB, the particles produced were Pd THH (161 ± 9 nm, 140 particles measured diagonally; histogram provided in Fig. S1†) with high monodispersity (>99% THH) (Fig. 1A). However, when the surfactant was changed to BioUltra B CTAB or BioXtra CTAB, the particles produced had CC morphologies (Fig. 1B and C). These two surfactants additionally generated samples that were only around 75% CC, along with multiply twinned side products such as rods and bipyramids.

### Analysis and testing of potential elemental contaminants

Iodide is a known CTAB contaminant, with lot-to-lot, product line, and manufacturer variations reported in the literature, and thus was of immediate interest as a possible cause of particle growth disparities resulting from the surfactant source.<sup>6–8,20</sup> Iodide is an important rate-determining ion in metal nanoparticle synthesis but its influence can be subtle and difficult to understand, as halides play numerous and complex roles in particle growth solutions. Halide ions can (1) slow metal precursor reduction by exchanging with other



**Michelle L. Personick**

*Michelle Personick is an associate professor in the Department of Chemistry at the University of Virginia (UVA). She received her BA from Middlebury College (2009) and her PhD from Northwestern University working with Prof. Chad Mirkin (2013). From 2013–2015, she was a postdoctoral researcher at Harvard University with Prof. Cynthia Friend and co-advised by Prof. Robert Madix. She began her independent career at*

*Wesleyan University in 2015 before moving to UVA in 2023. Her current research includes the development of *in situ* electro-analytical methods for understanding and designing materials syntheses as well as the application of precision nanomaterials in catalysis.*





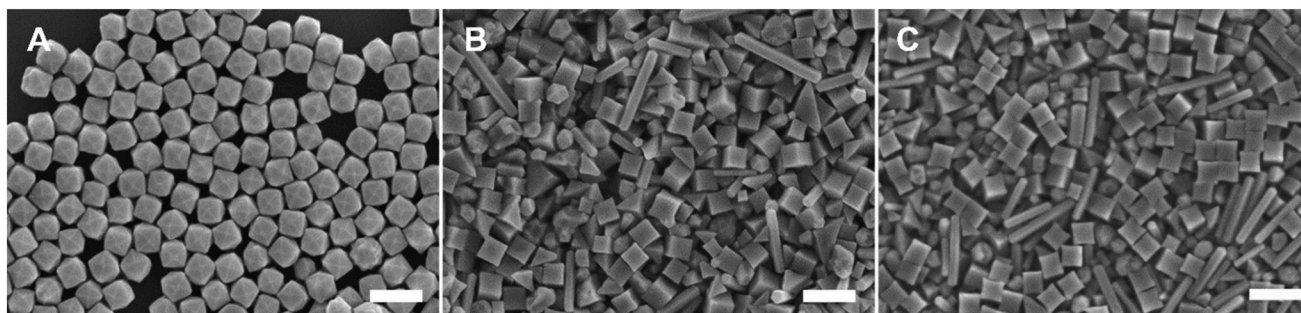


**Fig. 1** Scanning electron microscopy (SEM) images of Pd THH and CC. (A) Pd THH nanoparticles synthesized in BioUltra A CTAB. (B) Pd CC nanoparticles synthesized in BioXtra CTAB. (C) Pd CC nanoparticles synthesized in BioUltra B CTAB. Scale bars: 300 nm.

ligands on metal ions in solution and decreasing the reduction potential of the complex; (2) adsorb to and passivate specific nanoparticle facets to direct shape during growth; (3) slow growth by non-preferentially passivating all nanoparticle surfaces and blocking reduction at the surface; (4) cause pitting or change particle morphology *via* oxidative etching in the presence of oxygen; or (5) catalyze metal precursor reduction by aiding in metal ion binding to the metal nanoparticle surface.<sup>12,21,22</sup> Iodide in particular tends to be associated with significant shape changes, as the magnitude of halide ion effects in metal nanoparticle growth solutions is ordered according to increasing ion size and metal binding affinity ( $\text{Cl}^- < \text{Br}^- < \text{I}^-$ ).<sup>23–25</sup>

Elemental analysis *via* inductively coupled plasma mass spectrometry (ICP-MS) and IC was undertaken to understand and quantify any differences in the amount of multiple trace elemental contaminants, including iodide, across the three surfactant batches. Differences in elemental contamination were noted for Na, K, Ca, Fe, S, Cl, Br, and I across the three CTAB formulations (Table S1†). The ICP-MS and IC data—though not fully conclusive, as most elemental contaminant amounts were close to the limit of detection—suggest that the amount of iodide contamination is generally higher in BioUltra A than in BioUltra B or BioXtra. This is consistent with the literature, which has identified BioXtra as the MilliporeSigma CTAB variety with the least iodide.<sup>8</sup> BioUltra B and BioXtra were close enough to the limit of detection that conclusively ordering their individual levels of iodide contamination was difficult, but the two formulations appeared to have different small amounts of iodide.

To probe the possible influence of iodide, micromolar concentrations of NaI consistent with the measured differences in iodide concentration in the various CTAB sources were added to BioXtra-based growth solutions ( $0 < x < 2.90 \mu\text{M}$ , equivalent to  $0 < x < 300 \mu\text{L}$  0.1 mM NaI added, consistent with a calculated upper limit of  $2.78 \mu\text{M}$  or  $287 \mu\text{L}$  of 0.1 mM NaI, Table S2†). The addition of these small amounts of NaI notably changed product morphologies, indicating that iodide contamination at these low concentrations is sufficient to alter product formation. However, adding iodide to BioXtra CTAB was unable to replicate the THH produced in BioUltra

A. Instead, the products were TC and corner-truncated TC at moderate NaI concentrations ( $0.48\text{--}1.94 \mu\text{M}$ ), and rhombic dodecahedra (RD)—sometimes with truncations—at higher concentrations of NaI ( $1.94\text{--}2.90 \mu\text{M}$ ) (Fig. 2).

Similarly, a sizable iodide gradient in BioUltra B CTAB generated a series of products that again did not include any THH (Fig. S2†), instead transitioning directly from CC (Fig. S2B†) to TC (Fig. S2C†) to RD (Fig. S2D†). This gradient's products were also shifted in the CC-forming direction from those seen in the BioXtra iodide gradient at the same additive concentrations, confirming that the two have different levels of iodide contamination both from BioUltra A and from one another (Fig. 2B vs. Fig. S2B†). The fact that micromolar concentrations of NaI were sufficient for shape direction in BioXtra and

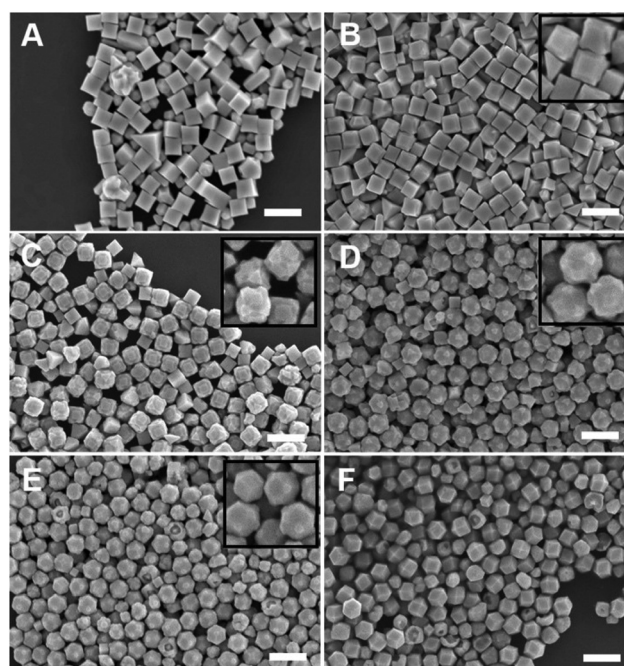


**Fig. 2** SEM images of Pd nanoparticle shape as a function of iodide concentration in BioXtra CTAB. (A) 0.24, (B) 0.48, (C) 0.97, (D) 1.45, (E) 1.94, and (F) 2.90  $\mu\text{M}$  added NaI in a standard growth solution that would produce THH in BioUltra A CTAB. Scale bars: 300 nm.



BioUltra B but were insufficient to provide a THH-forming condition suggests that iodide contamination could be part, but not all, of what is directing the differences in behavior between the various lots of CTAB.

Unlike the shape-directing effects seen with the addition of NaI to BioXtra, the addition of salts of Na, K, Ca, Fe, S, Cl, and Br—which had higher measured concentrations in BioXtra—into BioUltra A at concentrations consistent with and higher than those indicated by elemental analysis had little visible effect on product morphology (Fig. S3 and S4†). These results suggest that iodide contamination is likely the only relevant form of inorganic contamination that contributes to reproducibility issues for the THH synthesis. Additionally, they support the use of the sodium-halide salts for iodide addition experiments, as Na<sup>+</sup> ions were not associated with significant shape direction in the absence of I<sup>−</sup> anions.

### Electrochemical measurement of differences in reaction environment

Since an elemental inorganic impurity alone could not fully account for the morphological differences in products produced across the three surfactant sources, we employed our previously-reported electrochemical measurement approach to better understand the differences in chemical environment between the growth solutions.<sup>19</sup> Specifically, *in situ* open-circuit potential measurements of the solution potential of a colloidal synthesis and the change of this mixed potential throughout the reaction can provide insight into the strength of the reducing environment in which nanoparticles are forming. The open-circuit potentials of colloidal reactions under the standard THH synthesis conditions in each of the three different surfactant sources were measured in a three-electrode electrochemical cell for three hours. Product morphology was determined *via* scanning electron microscopy (SEM) after completion of the electrochemical measurement.

The open-circuit potential of the growth solution for the successful THH synthesis in BioUltra A CTAB was 0.52 V *vs.* standard hydrogen electrode (SHE) prior to the injection of Pd nanocube seeds and AA (Fig. 3). The addition of seeds and reducing agent caused the solution potential to rapidly drop to 0.30 V *vs.* SHE, and then the measured potential increased to 0.345 V *vs.* SHE over the three-hour measurement period. Most of the increase in potential (0.30 V *vs.* SHE to 0.33 *vs.* SHE) happened in the first ten minutes of the reaction, but the solution potential continued to gradually increase for the remainder of the three hours. The initial potentials of the BioUltra B and BioXtra growth solutions were quite similar to that of the BioUltra A growth solution, at about 0.515 V *vs.* SHE. However, following the injection of AA and seeds to initiate the redox reaction, the measured potentials began to differ, with the BioUltra B growth solution's potential dropping to 0.285 V *vs.* SHE and the BioXtra growth solution's potential decreasing to 0.24 V *vs.* SHE. The solution potentials for these reactions ultimately only increased to just above 0.30 V for BioUltra B and 0.29 V *vs.* SHE for BioXtra. These results indicate that, when combined with other components of the growth solution, both

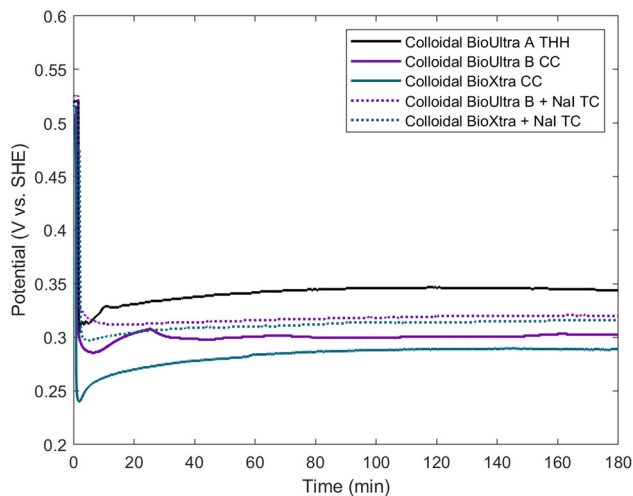


Fig. 3 Open-circuit potential measurements of colloidal syntheses in BioUltra A, BioUltra B, and BioXtra CTAB using the standard THH conditions, as well as growth solutions made in BioUltra B and BioXtra CTAB with 0.97  $\mu\text{M}$  added NaI.

the BioUltra B and BioXtra CTAB formulations lead to a stronger reducing environment (lower mixed solution potential) during Pd particle synthesis. In the colloidal particle synthesis literature, a stronger reducing environment is correlated with faster reaction kinetics,<sup>23,26</sup> indicating a possible difference in rates of metal ion reduction and nanoparticle growth between syntheses in the different CTAB sources. The stronger reducing environment and faster growth kinetics could in turn lead to generation of the CC products and twinned side products, as opposed to the THH grown in BioUltra A with an otherwise identical set of reagents and concentrations.

Returning to the NaI gradient experiments, 0.97  $\mu\text{M}$  NaI generated corner-truncated TC (which are somewhat similar to THH, with a small cubic protrusion developing rather than a fully formed pyramid on each cubic face) in both BioUltra B (Fig. S2C†) and BioXtra CTAB (Fig. 2C). The open-circuit potentials of growth solutions containing this concentration of iodide in both BioUltra B and BioXtra CTAB were therefore measured and compared to THH-forming conditions in BioUltra A CTAB (Fig. 3). The two growth solutions with added iodide had similar solution potentials to BioUltra A prior to the addition of AA, at 0.525 V *vs.* SHE for BioUltra B and 0.52 V *vs.* SHE for BioXtra. After the addition of the reducing agent and seeds, the BioUltra B and BioXtra solution potentials decreased to 0.31 V *vs.* SHE and 0.30 V *vs.* SHE respectively. The two solution potentials did not change as much in the subsequent initial minutes of the reaction, instead staying relatively constant over the three hours of the measurement and ultimately reaching similar values of 0.32 V *vs.* SHE for BioUltra B and 0.315 V *vs.* SHE for BioXtra. This suggests that the addition of iodide slows the initial rate of change of the solution potential as compared to the three syntheses in unmodified CTAB. Although iodide addition raises the overall solution potential during the reaction compared to that of the



syntheses in unmodified BioUltra B or BioXtra, the solution potential is still lower (more strongly reducing) than that of BioUltra A. As these iodide addition conditions represent the best shaped products (*i.e.* the closest to THH) seen with NaI concentration gradients in BioUltra B and BioXtra CTAB, these results expand on what was observed with SEM—that the inclusion of iodide in the growth solution may help facilitate shape formation but is not sufficient to match the BioUltra A THH growth conditions—and add that the remaining gap is due to differences in the strength of the reducing environment. Some non-elemental contaminant, possibly along with iodide, must be the cause of the kinetic differences leading to difficulties in THH replication.

### Correlating reducing environment strength and shape development in the THH synthesis

These electrochemical measurements imply a significant influence of the reducing environment across reactions in the different CTAB varieties, suggesting that the THH form at a specific local kinetic optimum. Therefore, we explored what happens to product morphology in BioUltra A CTAB if the strength of the reducing environment is intentionally modified by changing the ratio of  $[\text{Pd}^{2+}]$ : $[\text{AA}]$  while holding one of these two concentration variables constant. This control of solution potential alters metal ion reduction rates and particle growth kinetics. Varying the concentration of  $\text{Pd}^{2+}$  ions in the growth solution in BioUltra A CTAB while maintaining a constant AA concentration of 0.96 mM resulted in drastic changes in par-

ticle morphologies (Fig. 4). At the highest concentration of Pd precursor tested (0.47 mM  $\text{Na}_2\text{PdCl}_4$ ), cubic products formed, along with a minor subpopulation of multiply twinned side products, such as bipyramids and rods (Fig. 4A). As the concentration of Pd precursor was decreased, the particles formed were TC with a single  $\{100\}$  terrace feature on each of their square side faces (Fig. 4B). As the metal concentration was further decreased, high-index  $\{hk0\}$  facets developed, changing the flat  $[100]$  terraced features of the TC into pointed pyramidal features, consistent with a THH shape (Fig. 4D). Lower concentrations of metal caused the particles to lose their convex high-index surfaces, eventually generating CC with truncated corners (Fig. 4F). Interestingly, the convex THH to CC shape transition does not appear to go through a fully platonic cubic intermediate, but rather an intermediate where the pseudocubic products have both concave and convex features at the same time (Fig. 4E).

Open-circuit potential measurements of the colloidal TC-, THH-, and CC-forming conditions (0.38 mM, 0.24 mM, and 0.15 mM  $\text{Na}_2\text{PdCl}_4$  in solution, respectively) reveal a direct relationship between the metal concentration and solution potential over the time course of each synthesis (Fig. 4G). The initial solution potentials prior to the introduction of reducing agent differed noticeably, with higher concentrations of  $\text{Pd}^{2+}$  yielding a higher starting potential. Following the introduction of reducing agent and seeds, the high  $[\text{Pd}^{2+}]$  and low  $[\text{Pd}^{2+}]$  solution potentials all dropped significantly, but not to the same value, instead retaining their initial ordering. The slopes

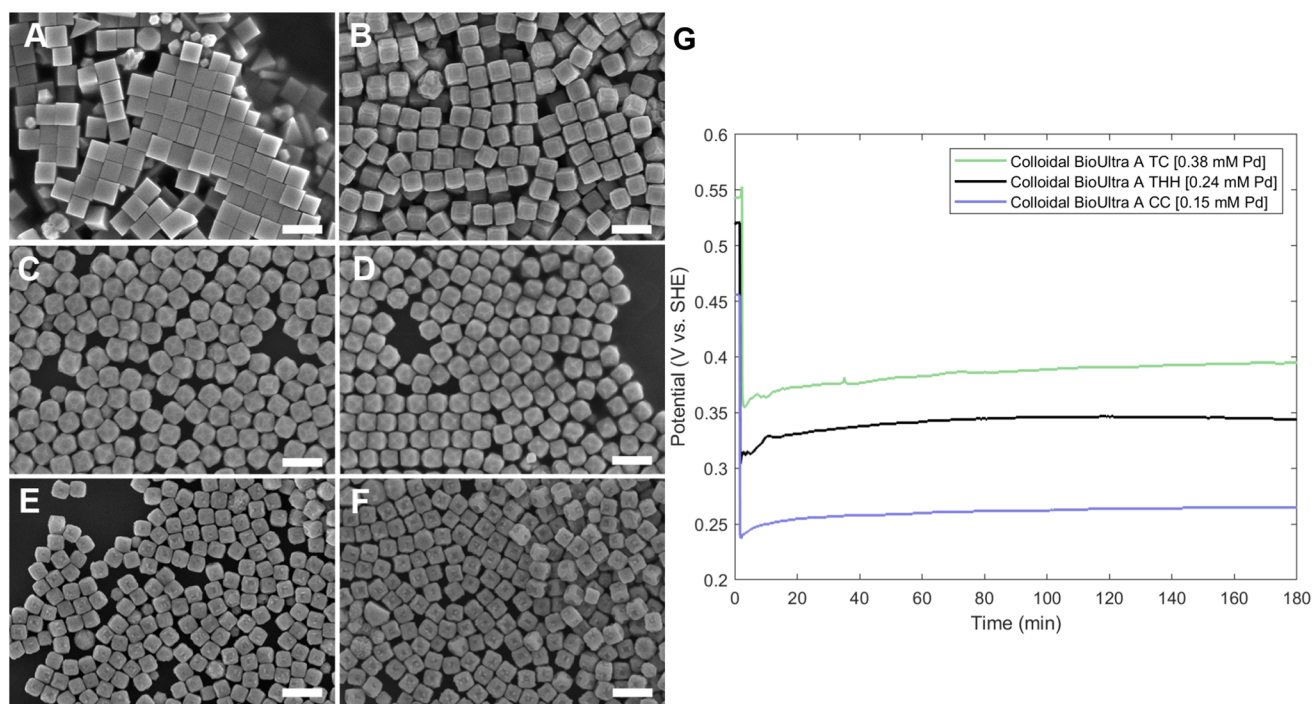


**Fig. 4** (A–F) SEM images of Pd nanoparticle shape as a function of metal ion concentration. Gradient of  $\text{Pd}^{2+}$  concentration in BioUltra A CTAB with (A) 500, (B) 400, (C) 350, (D) 250, (E) 200, and (F) 150  $\mu\text{L}$  of 10 mM  $\text{Na}_2\text{PdCl}_4$ . These volumes correspond to overall concentrations of (A) 0.47, (B) 0.38, (C) 0.34, (D) 0.24, (E) 0.19, and (F) 0.15 mM  $\text{Na}_2\text{PdCl}_4$ . (G) Open-circuit potential measurements of reactions with 0.38 mM (B), 0.24 mM (D) and 0.15 mM (F) of  $\text{Pd}^{2+}$  in growth solution. Scale bars: 300 nm.





of the change in open-circuit potential over the course of the reaction for the three metal concentrations measured are almost identical, but the magnitude of solution potential remains notably different between each solution. In contrast to the solution potential of around 0.345 V *vs.* SHE measured at reaction completion in the standard THH growth solution, the high  $[Pd^{2+}]$  and low  $[Pd^{2+}]$  solutions have final potentials of around 0.395 V *vs.* SHE and 0.265 V *vs.* SHE after three hours, respectively. A comparison of the three open-circuit potential traces suggests that lower concentrations of metal precursor relative to the constant concentration of AA lead to faster reaction kinetics through a stronger reducing environment.

An alternative way to modify the colloidal solution potential is by tuning the concentration of the reducing agent (AA) while holding the concentration of the Pd precursor constant. AA has successfully been used as a shape-control agent in a similar Pd particle synthesis to produce a shape gradient including RD, TC, and cubes with increasing [AA] and/or decreasing [CTAB].<sup>27</sup> The standard concentration of AA used to successfully produce the THH in BioUltra A, 0.96 mM, is in four-fold excess relative to the concentration of metal ions in the growth solution (0.24 mM). Concentrations of AA as low as 0.24 mM—stoichiometrically equivalent to the concentration of the Pd precursor—still produced high quality THH particles (Fig. S5A–C†). Increasing the AA concentration, however, caused the particle quality to decrease, yielding bumpy, overgrown THH particles (Fig. S5D and S5E†). As the AA concentration was further increased, bumpy cubes with somewhat concave surfaces were produced (Fig. S5F†), similar to conditions with low concentrations of metal precursors. The role of AA concentration further illustrates the subtle local reaction rate optimum required to produce the THH particles, suggesting a key role of specific reaction rate in shape determination. Interestingly, samples with the same  $[Pd^{2+}]:[AA]$  ratios do not display the same product morphologies when the ratio is manipulated through changing  $[Pd^{2+}]$  *vs.* changing [AA] from the standard conditions (1:2  $Pd^{2+}:AA$ , Fig. S5B† *vs.* Fig. 4A; 1:6  $Pd^{2+}:AA$ , Fig. S5D† *vs.* Fig. 4F), indicating a possible unique role of  $Pd^{2+}$  concentration in directing shape. Nitric acid concentration, which can be involved in controlling the reactivity of ascorbic acid by changing solution pH, was also studied but had a more subtle effect, mostly determining THH quality rather than particle shape (Fig. S6†).

### Benchmarking colloidal results and measurements against electrodeposition

To establish the relevance of the measured solution potentials of the THH-forming conditions in understanding and troubleshooting particle growth, we employed our previously-reported approach for replication of colloidal particle synthesis on an electrode surface to develop a constant-current electrochemical synthesis of monometallic Pd THH and additional shapes from a  $[Pd^{2+}]$ -dependent shape gradient.<sup>19</sup> This electrodeposition synthesis, where the chemical reducing agent was replaced with applied current, was optimized empirically. The

composition of the electrochemical growth solution was very slightly adapted from the colloidal BioUltra A THH growth solution. Ascorbic acid was omitted and 1  $\mu$ L of an undiluted Pd nanocube seed colloid was drop-cast and dried onto a glassy carbon electrode (GCE) surface rather than injecting seeds directly into the growth solution. An initial selection of application of  $-3.82 \mu A cm^{-2}$  applied current for 30 minutes was made based on insight from the development of our group's previously-published synthesis of Pd icosahedra.<sup>19</sup> Iterative changes in both applied current and reaction duration in response to morphological observations revealed that decreasing the magnitude of the current to around  $-2.04 \mu A cm^{-2}$  was required to produce THH rather than products shifted toward RD, and that a three-hour reaction time was necessary for optimal particle morphology.

From the electrodeposition conditions for THH, the concentration of  $H_2PdCl_4$  was modified to replicate the colloidal gradient of shape *vs.*  $[Pd^{2+}]$  while holding all other chemical and electrochemical conditions constant. Changing the concentration of the  $Pd^{2+}$  source,  $H_2PdCl_4$ , in the electrodeposition growth solution from 0.24 mM (consistent with the colloidal THH growth solution) to 0.12 mM produced better-formed THH, likely because the limited size of the GCE necessitates deposition of fewer seeds than in the colloidal case (Fig. 5B). The addition of 0.30 mM or higher concentrations of metal precursor generated RD (Fig. 5A). A decrease in  $[Pd^{2+}]$  to 0.061 mM gave CC products (Fig. 5C). This is consistent with the appearance of CC products at low metal concentrations colloidal, and supports the hypothesis that higher ratios of electron supply (due to either applied current magnitude or chemical reductant concentration) to metal precursor have the same effects on particle growth rate, as identified by product morphology, in both the colloidal and electrochemical cases. Metal concentrations of 0.048 mM and lower were too low to yield well-formed products, leading to small, indistinct particles. With an intermediate metal concentration of 0.073 mM, products underwent a concave-to-convex transition that produced particles with concave faces with substantial protrusions (Fig. S7A†), providing interesting mechanistic insight into the shape transition, which, like the colloidal case (Fig. S7B† and Fig. 4E), does not appear to go through a perfectly cubic structure between the CC and THH morphologies.

Chronopotentiometry measurements of the CC, THH, and RD electrodeposition conditions were undertaken to compare the electrochemical and colloidal synthesis results (Fig. 5D). Chronopotentiometry and open-circuit potential measurements can be directly compared to understand time-resolved changes in solution potential.<sup>19</sup> The initial potentials were similar for CC- and THH-forming electrodeposition conditions and higher for RD (0.061 mM, 0.12 mM, and 0.30 mM metal precursor, respectively). Following the application of current, the potentials for the electrodeposition of CC, THH, and RD drop to 0.21 V *vs.* SHE, 0.27 V *vs.* SHE, and 0.32 V *vs.* SHE, respectively. The potential for the THH-forming condition subsequently rises more sharply than the RD-forming solution, ultimately ending at similar potentials (0.42 V *vs.* SHE for the



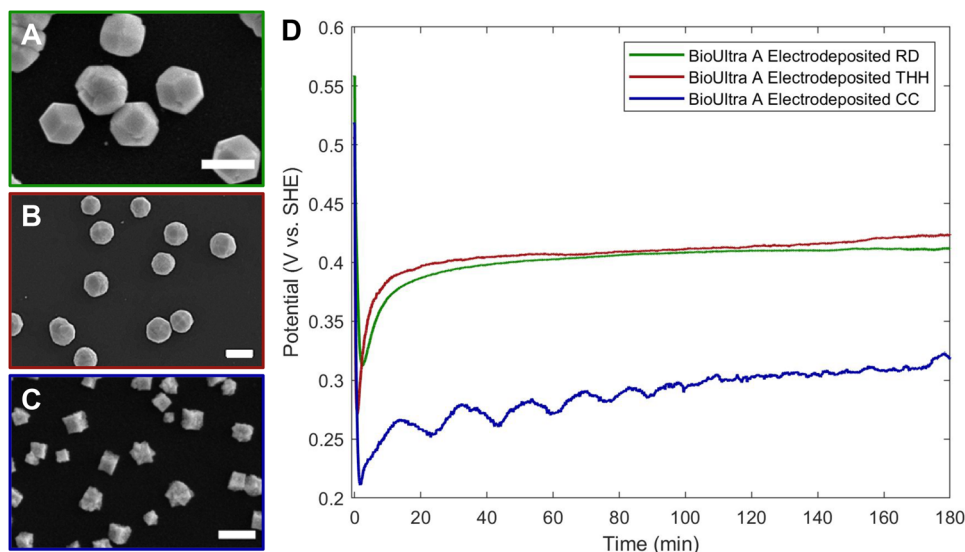


Fig. 5 SEM images of electrodeposited (A) RD (0.30 mM Pd<sup>2+</sup>), (B) THH (0.12 mM Pd<sup>2+</sup>), (C) CC (0.061 mM Pd<sup>2+</sup>), and (D) chronopotentiometry measurements of each electrodeposition synthesis. Scale bars: 300 nm.

THH and 0.41 V vs. SHE for the RD). The CC electrodeposition, as expected, has a more strongly reducing potential than the higher [Pd<sup>2+</sup>] reactions, increasing from 0.21 V to 0.27 V vs. SHE in the first 15 minutes of the reaction and then further increasing to 0.32 V vs. SHE over the remainder of the three hours. The CC chronopotentiometry trace displays some cyclic noise that may be indicative of mass transport limitations and/or depletion of available metal precursor near the electrode interface due to the low overall concentration of [Pd<sup>2+</sup>] in the solution.

Replication of this [Pd<sup>2+</sup>]-mediated electrodeposition shape gradient in BioUltra B CTAB with all conditions kept otherwise identical to those of the BioUltra A was not successful (Fig. S8†). While low metal concentrations (0.061 mM) of metal once again generated small pseudocubic particles with slight concavities, they were not as concave as the BioUltra A CC and were accompanied by a wider variety of side products. Growth solutions containing 0.24 mM and 0.30 mM metal precursor both led to poorly-formed pseudo-THH in a 1 : 3 ratio with multiply-twinned side products, indicating less precise control of the reaction with this CTAB lot, as well as some shifting of the concentration-based shape gradient; 0.30 mM Pd precursor generates well-formed RD in BioUltra A CTAB. Electrodeposition from a growth solution made with 0.48 mM Pd<sup>2+</sup> led to large, poorly-formed particles. Chronopotentiometry measurements of these unsuccessful syntheses in BioUltra B revealed a stronger reducing environment at each [Pd<sup>2+</sup>] than those of the analogous experiments in BioUltra A (Fig. S8E†).

The persistence of lot-to-lot differences in CTAB solutions during electrodeposition implies a fundamental difference between BioUltra A's and BioUltra B's kinetic control of the growth solution, such as a difference in viscosity (leading to diffusion limitations), surface passivation of the growing nanoparticles (which could be magnified in the electrochemical

case due to charge interactions with the electrode), or structural changes in CTAB bilayer or micelle formation near particle surfaces, any of which could in turn be affected by differing purities. While the different CTAB lots and lines do exhibit different solution pH values at 50 mM (Table S3†), the lack of success of the BioUltra B shape gradient *via* electrodeposition implies that pH differences and/or the presence of an impurity leading to differences in buffering behavior between the lots and lines of CTAB is not the fundamental issue, as the protonation state and pH-dependent activity of ascorbic acid are not at play in the electrochemical case. Regardless, contaminant differences in surfactant are in some way responsible for changing reaction kinetics even when the rate of electron supply is held constant.

The chronopotentiometry measurements of the electrochemical CC and THH syntheses in BioUltra A were compared to the colloidal THH made in BioUltra A and colloidal CC formed under THH conditions in BioUltra B and BioXtra to understand whether the electrodeposition syntheses represent a useful benchmark. Open-circuit potential measurements of the BioUltra A colloidal standard THH synthesis and the standard synthesis conditions with BioUltra B and BioXtra CTAB sources, which morphologically produce CC, all fell in between the electrochemical THH and CC in potential (Fig. S9†). The colloidal synthesis in BioUltra A CTAB has a more similar magnitude of potential and kinetics to the electrochemical THH, while the colloidal syntheses in BioUltra B and BioXtra have lower solution potentials that are more similar to the electrochemical CC.

#### Identifying the remaining impurity and establishing reproducible synthesis

After ruling out elemental impurities as the single source of product-to-product and lot-to-lot differences in CTAB behavior





and establishing solution potential as a key factor in controlling particle shape, multiple avenues were explored to account for molecular impurities that could lead to the differences in solution potential and product formation. Chain-length irregularities in the hydrocarbon tail of each CTAB sample were not conclusively identifiable *via* high-resolution mass spectrometry or NMR. To better control possible sources of contamination, CTAB was directly synthesized from cetyl bromide and trimethylamine in an attempt to understand possible routes of impurity introduction (Scheme S1†). The resulting CTAB product had both acetone and methanol contamination from recrystallization (confirmed *via* NMR, Fig. S10†). The kinetic implications of this solvent contamination were underscored by the particle morphologies obtained when the synthesized CTAB was used in colloidal synthesis. Growth solutions made with the synthesized CTAB produced octahedral nanoparticles (Fig. S11†) under both standard THH forming synthetic conditions and in a growth solution with 0.33 mM Pd<sup>2+</sup> (all other conditions standard). The absence of octahedra from the typical [Pd<sup>2+</sup>]-mediated shape gradient in BioUltra A and from the iodide addition shape gradients in BioUltra B or BioXtra implies that the solvent contamination produces unique shape-directing rate effects. These could be related to specific

adsorption of solvent contaminants on the growing particle surface, to the diffusion rate of solution components because of the change in solution viscosity, or to differences in local CTAB concentration or structural arrangement that affect micelle formation and/or surface passivation.

As a result of the relevance of the appearance of solvent contamination in the synthesized CTAB and its shapedirecting influence in nanoparticle synthesis, NMR spectra were also obtained for BioUltra B and BioXtra CTAB (<sup>1</sup>H NMR, 600 MHz, D<sub>2</sub>O; NMR data available in ESI†). These spectra show a chemical shift not indicative of pure CTAB at 2.23 ppm (Fig. 6). This signal corresponds to the 2.22 to 2.23 ppm value of the methyl proton signal of acetone in D<sub>2</sub>O.<sup>28</sup> Drying the as-received powdered CTAB in an oven at 80 °C for 24 hours led to elimination of the unexpected signal, indicating possible solvent contamination of the BioXtra and BioUltra B CTAB formulations. No powdered BioUltra A was available at the time when NMR spectra were obtained; NMR taken of BioUltra A in solution in DI water (with 10% D<sub>2</sub>O) had such poor signal relative to the size of the solvent peak that identification of any possible solvent impurities was inconclusive (Fig. S12†).

Empirical synthetic development *via* concentration gradients of NaI, acetone, and Pd<sup>2+</sup> was sufficient to establish a pro-

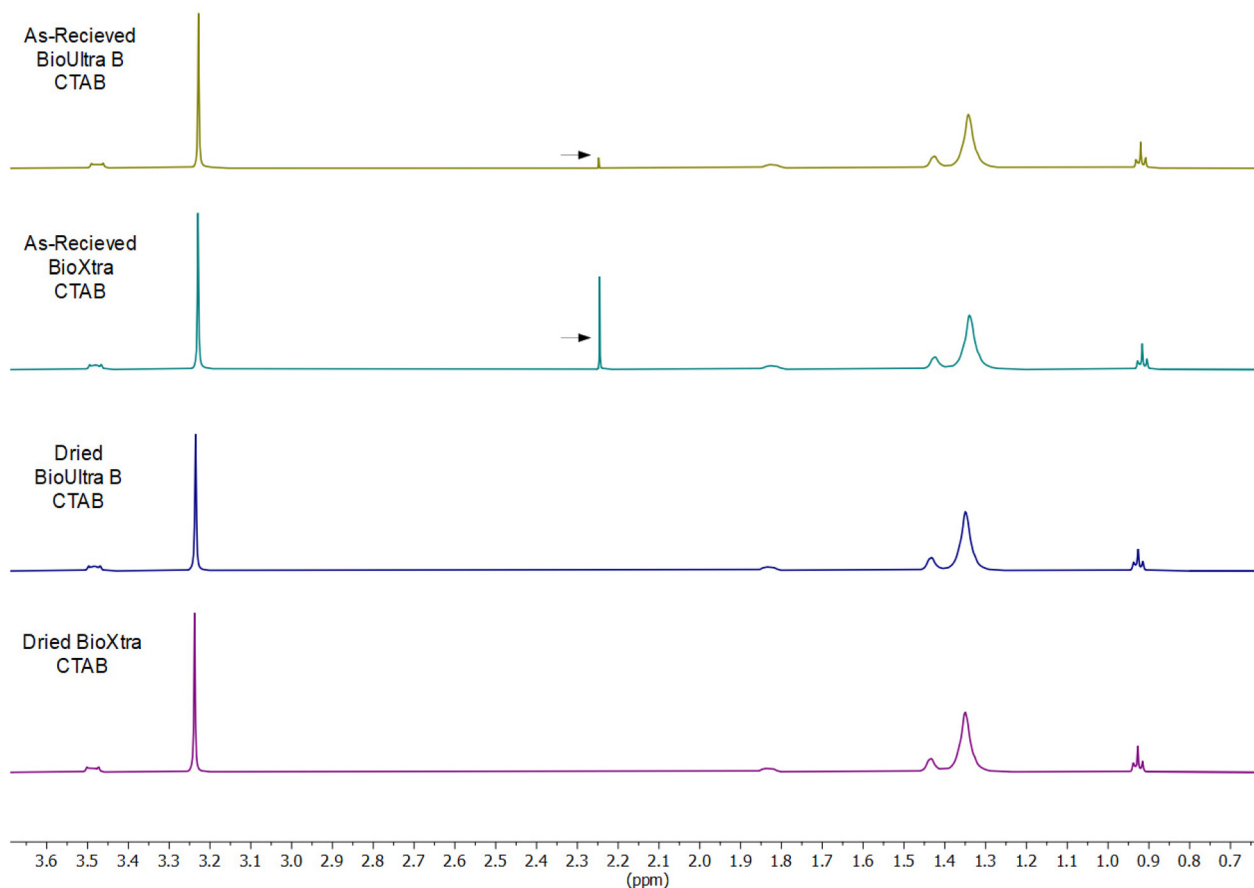


**Fig. 6** Comparison between <sup>1</sup>H NMR spectra for various formulations of as-received and dried CTAB. Arrows indicate possible acetone peaks in as-received BioUltra B and BioXtra CTAB.



protocol for synthesis of well-formed THH and replication of the desired  $[\text{Pd}^{2+}]$ -based shape gradient in BioUltra B CTAB. Addition of  $0.68 \mu\text{M}$  NaI and  $50 \mu\text{L}$  of neat acetone ( $0.068 \text{ M}$  in the growth solution) into a standard growth solution successfully produced THH (Fig. S13B†). Lower and higher concentrations of iodide were found to produce corner-truncated TC and RD respectively (Fig. S13†). While the use of an organic solvent as a shape-directing agent in a particle synthesis is unusual in aqueous solution, organic solvents are known in the literature to interact with surfactants and similarly-structured phospholipid molecules as both cosolvents with and contaminants in water. They affect formation of, size of, and degradation of micelles and bilayer membranes. Specifically, at the low concentrations considered here, amphiphilic solvent molecules are likely to intercalate between charged surfactant headgroups, with their polar ends sitting between or just below headgroups and nonpolar portions sitting between hydrocarbon tails. This can increase the size of micelles and cause more disorder and/or patterns of interdigitation in hydrocarbon tails.<sup>29–41</sup> Solvent molecules in even low concentrations can also cause chaotropic effects that can affect the behavior of micelles and bilayers, and presumably also of other solutes.<sup>29,33</sup>

Generalizability of the acetone and iodide adjustment scheme to all batches of BioUltra CTAB was achieved by oven-drying the as-received BioUltra B powder at  $80$  to  $100 \text{ }^\circ\text{C}$  for 24 hours. Modification of a dried BioUltra B-based growth solution with  $0.68 \mu\text{M}$  NaI and between  $190 \mu\text{L}$  and  $270 \mu\text{L}$  of acetone ( $0.26 \text{ M}$  to  $0.36 \text{ M}$  in the growth solution) was sufficient to produce THH under otherwise standard conditions (Fig. S14†). Optimal THH were produced with  $0.68 \mu\text{M}$  NaI and  $190 \mu\text{L}$  of acetone ( $141 \pm 12 \text{ nm}$ , 145 particles measured diagonally; Fig. S15A†). The formation of the THH shape was confirmed *via* higher-magnification scanning transmission electron microscopy (STEM) as well as SEM imaging (Fig. S16A–D†). The full  $[\text{Pd}^{2+}]$ -based shape gradient originally demonstrated in BioUltra A CTAB can be replicated in BioUltra B modified with  $0.68 \mu\text{M}$  NaI and  $190 \mu\text{L}$  of acetone ( $0.26 \text{ M}$  in the growth solution) (Fig. 7). This shape gradient displays morphologies roughly equivalent to those in Fig. 4 with some minor differences in particle quality. Variation of acetone and/or iodide addition outside this range causes loss of one or more of the expected shapes due to shifting of the gradient, leading to the conclusion that these are the most optimal concentrations for these additives. The products of an iodide gradient in a growth solution with the optimized  $190 \mu\text{L}$  of acetone were, as expected, shifted with respect to the iodide concentration at which specific shapes form when compared to the iodide gradient in BioUltra B without optimal acetone (Fig. S2†), but they exhibited an analogous transition from cubes (Fig. S17A†) to TC (Fig. S17B†) to RD with increasing added iodide (Fig. S17C and D†). Of note are the appearance of TC at the iodide concentration closest to the THH-forming condition ( $0.48 \mu\text{M}$  NaI for TC *vs.*  $0.68 \mu\text{M}$  NaI for THH), as well as the truncated octahedral products at the highest two iodide additive concentrations (Fig. S17E and F†), which

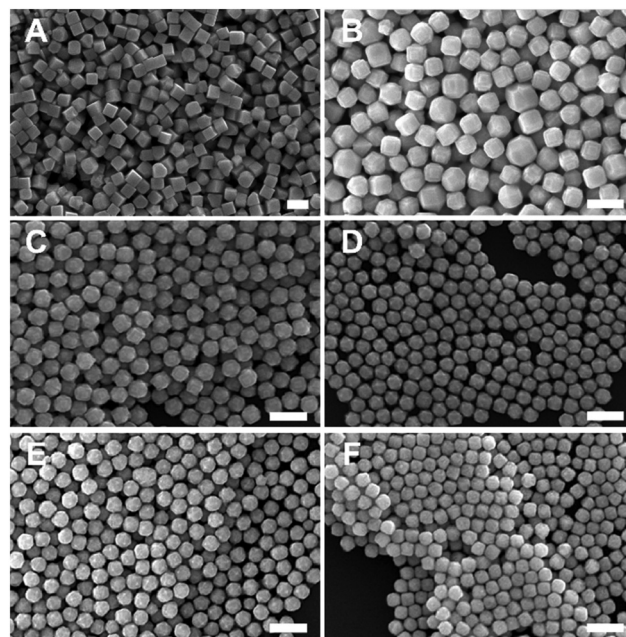


**Fig. 7** SEM images of Pd nanoparticle shape as a function of  $\text{Pd}^{2+}$  concentration in dried BioUltra B CTAB modified with  $0.68 \mu\text{M}$  NaI and  $190 \mu\text{L}$  of acetone ( $0.26 \text{ M}$  in the growth solution). Samples contain (A)  $500$ , (B)  $400$ , (C)  $350$ , (D)  $250$ , (E)  $200$ , and (F)  $150 \mu\text{L}$  of  $10 \text{ mM}$   $\text{Na}_2\text{PdCl}_4$ . These volumes correspond to overall concentrations of (A)  $0.47$ , (B)  $0.38$ , (C)  $0.34$ , (D)  $0.24$ , (E)  $0.19$ , and (F)  $0.15 \text{ mM}$   $\text{Na}_2\text{PdCl}_4$ . Scale bars:  $300 \text{ nm}$ .

match literature reports of a related morphology in growth solutions modified with moderate to high iodide concentrations.<sup>42</sup> Smaller TC particles were also produced in BioUltra B using the optimal additive concentrations with either a twenty-fold ( $70 \pm 7 \text{ nm}$ , 154 particles measured diagonally) or forty-fold ( $45 \pm 7 \text{ nm}$ , 146 particles measured diagonally) increase in the concentration of seed colloid added to the growth solution (Fig. S18†). Production of fully formed THH with high-energy tip features was not possible at this smaller size.

A THH synthesis in as-received BioXtra CTAB could not be optimized through addition of NaI and acetone. We posit that this difficulty was due to a higher amount of solvent contamination in as-received BioXtra compared to BioUltra B. Oven-drying of BioXtra CTAB for synthesis optimization was therefore necessary. Modification of a dried BioXtra CTAB-based standard growth solution with  $0.63$  to  $0.73 \mu\text{M}$  NaI and  $175$  to  $200 \mu\text{L}$  of acetone ( $0.24 \text{ M}$  to  $0.27 \text{ M}$  in the growth solution)—conditions that form THH in BioUltra B—yielded a mixture of corner-truncated TC (Fig. S14A, B, E and F†). When dried BioXtra was modified with  $0.77$  to  $0.92 \mu\text{M}$  NaI and  $150$  to  $300 \mu\text{L}$  of acetone ( $0.20 \text{ M}$  to  $0.40 \text{ M}$  in growth solution), results were RD, with some truncations at lower iodide concentrations (Fig. S19†). High iodide growth solutions have previously been reported as an RD-stabilizing condition for Pd nanoparticles in the literature;<sup>42</sup> high iodide concentrations without solvent also produced RD in as-received BioUltra B CTAB (Fig. S2F†). Empirical optimization of the dried BioXtra



solution eventually demonstrated that replication of both the standard THH synthesis ( $134 \pm 11$  nm THH, 119 particles measured diagonally; Fig. S15B†) and the surrounding  $[\text{Pd}^{2+}]$ -mediated shape gradient were possible with addition of  $0.58 \mu\text{M}$  NaI and  $230 \mu\text{L}$  of acetone ( $0.31$  M in the growth solution), but not at any other combination of additive concentrations tested (Fig. 8). The product morphologies in this dried, doubly-modified BioXtra growth solution (Fig. 8) show good agreement with those in BioUltra A (Fig. 2). The THH morphology was further confirmed *via* STEM imaging (Fig. S16E–H†). Comparison of the similar morphologies of TC made in as-received BioXtra with  $0.58 \mu\text{M}$  NaI and no added acetone and TC made in dried BioXtra with  $0.58 \mu\text{M}$  NaI and excessive acetone ( $340 \mu\text{L}$  of acetone, or  $0.46$  M in growth solution) supports the conclusion that as-received BioXtra has an overly high level of solvent contamination for formation of THH (Fig. S20†). An iodide gradient (Fig. S21†) in BioXtra CTAB with the optimal amount of acetone ( $230 \mu\text{L}$  or  $0.31$  M) added to the growth solution showed good morphological parity with the same gradient in BioUltra B (Fig. S17†), demonstrating TC/truncated THH (Fig. S21B†) at the closest iodide condition to the optimal THH forming concentration ( $0.48 \mu\text{M}$  NaI for TC *vs.*  $0.58 \mu\text{M}$  NaI for THH), as well as a progression to RD and truncated octahedra with excess iodide (Fig. S21C–F†), as expected. This confirms that iodide has the same effect across CTAB varieties once the as-received CTAB has been dried and the appropriate amount of acetone added to correct for differences in solvent contamination.

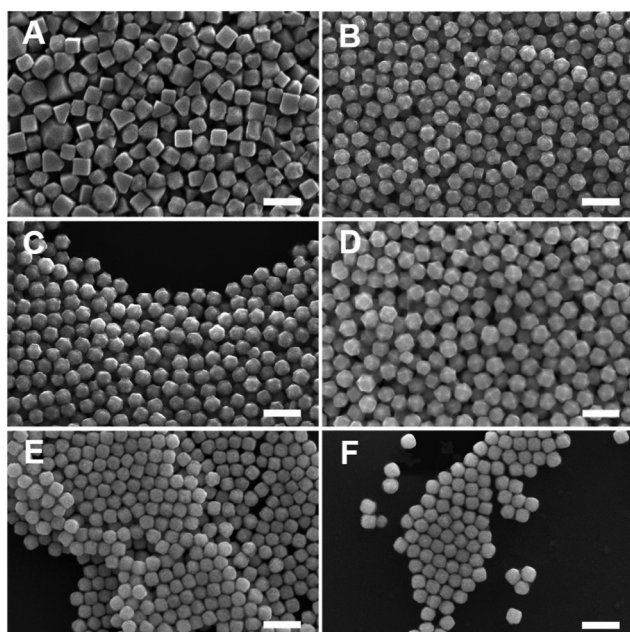


**Fig. 8** SEM images of Pd nanoparticle shape as a function of  $\text{Pd}^{2+}$  concentration in dried BioXtra CTAB modified with  $0.58 \mu\text{M}$  NaI and  $230 \mu\text{L}$  of acetone ( $0.31$  M in the growth solution). Samples contain (A) 500, (B) 400, (C) 350, (D) 250, (E) 200, and (F) 150  $\mu\text{L}$  of  $10$  mM  $\text{Na}_2\text{PdCl}_4$ . These volumes correspond to overall concentrations of (A)  $0.47$ , (B)  $0.38$ , (C)  $0.34$ , (D)  $0.24$ , (E)  $0.19$ , and (F)  $0.15$  mM  $\text{Na}_2\text{PdCl}_4$ . Scale bars:  $300$  nm.

### Confirmation of successful impurity identification using electrochemistry

Comparison of the open-circuit potential measurements of the doubly-modified dried BioUltra B and BioXtra THH and the standard BioUltra A THH reaction was undertaken to verify that these three THH formations occur at the same kinetic minimum and to understand any differences between the reactions. Interestingly, the dried, modified BioUltra B growth solution has a notably higher potential than the dried, modified BioXtra or BioUltra A growth solutions prior to the initiation of redox chemistry, but the potentials of the three solutions are otherwise similar over the course of the reaction after metal reduction begins (Fig. 9). The good agreement of the three potential traces following the introduction of reducing agent indicates parity between the reducing environment and reaction kinetics of the standard reaction in the original BioUltra A CTAB and the modified growth solutions in the two dried surfactants. This result also provides validation for the use of open-circuit potential measurements of colloidal syntheses as a means of benchmarking the optimal chemical growth solution conditions for successful synthesis of a given nanoparticle morphology, and for comparing and troubleshooting syntheses conducted with different lots of reagents or in different laboratories.

To explore the possibility of using open-circuit potential measurements for comparison of new synthetic conditions to a benchmark, we synthesized particles in CTAB purchased from Thermo Scientific (99%) and Tokyo Chemical Industries (TCI; 98.0%) using standard conditions. These two surfactants had not been studied in any of our previous experiments. The particles produced with these new CTAB sources were morphologically poor and quite different from one another, with the Thermo Scientific CTAB yielding small cubes and CC along

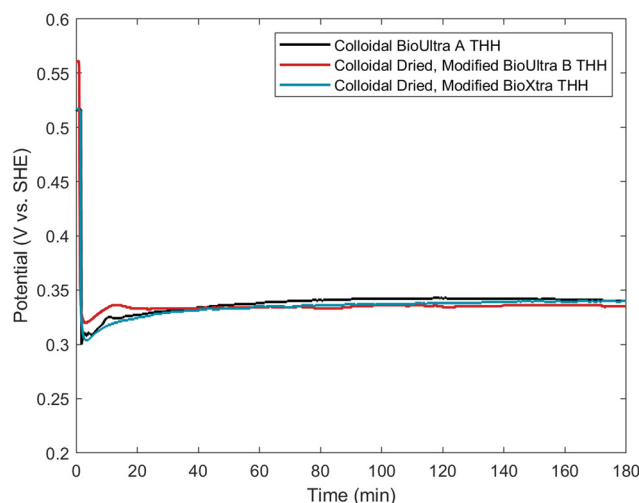


**Fig. 9** Comparison of the open-circuit potential measurements of the standard THH-forming conditions in BioUltra A CTAB, in dried BioUltra B CTAB modified with  $0.68 \mu\text{M}$  NaI and  $190 \mu\text{L}$  of acetone ( $0.26$  M in the growth solution), and in dried BioXtra CTAB modified with  $0.58 \mu\text{M}$  NaI and  $230 \mu\text{L}$  of acetone ( $0.31$  M in the growth solution).





with large poorly-formed particles, while the TCI CTAB led to formation of small cubes (Fig. S22A and S23A†). Samples of both new CTAB sources were oven-dried for further study.

Open-circuit potential measurements were taken of the standard reaction conditions in both new CTAB sources as received and the measurements were compared to the benchmark BioUltra A THH measurement (Fig. S22D and S23D†). This comparison showed that the mixed potential of the standard synthesis conditions in as-received Thermo Scientific CTAB was too strongly reducing relative to the successful benchmarked conditions for producing THH, and instead the measurement for this new CTAB matched very well with the open-circuit measurement for the as-received BioXtra CC, despite the different product morphologies. Based on this information, acetone and iodide concentrations identical to those used to produce THH in BioXtra (0.58  $\mu\text{M}$  NaI and 230  $\mu\text{L}$  of acetone (0.31 M in the growth solution)) were added to a growth solution made from oven-dried Thermo Scientific CTAB. These conditions were successful in producing truncated THH and TC particles (Fig. S22B†). Slightly decreasing the acetone and iodide additive concentrations (0.48  $\mu\text{M}$  NaI and 220  $\mu\text{L}$  of acetone (0.30 M in the growth solution)) improved the quality of the THH (Fig. S22C†). The open-circuit potential measurement for the growth solution in as-received TCI CTAB, meanwhile, showed a mixed potential that was significantly more positive than what is required for THH production. Typical iodide concentrations (0.58  $\mu\text{M}$  NaI) were then added to a growth solution made from dried TCI CTAB, but a lower acetone additive concentration was used (100  $\mu\text{L}$  of acetone (0.14 M in the growth solution)), since acetone has a strong effect on increasing the mixed potential of the growth solution. The particles that resulted from these modifications

were also TC/truncated THH (Fig. S23B†). Again, a slight decrease in the acetone and iodide additive concentrations (0.48  $\mu\text{M}$  NaI and 90  $\mu\text{L}$  of acetone (0.12 M in the growth solution)) was sufficient to optimize formation of THH (Fig. S23C†). Comparison of the open-circuit potential traces for THH formation in dried, modified Thermo Scientific and TCI CTAB to the BioUltra A CTAB benchmark showed good agreement (Fig. S22D and S23D†). These results validate the utility of open-circuit potential measurements as benchmarks to streamline troubleshooting and increase reproducibility in colloidal nanoparticle synthesis.

As a further test of the ability of solvent additives to mediate kinetic conditions through indirect control of solution potential, the acetone and iodide adjustment scheme was used in an electrochemical synthesis. Electrodeposition of THH in dried BioUltra B CTAB was achieved by maintaining the conditions used to generate THH in BioUltra A (0.12 mM metal in the growth solution;  $-2.04 \mu\text{A cm}^{-2}$  applied current for 3 hours) and adding 0.68  $\mu\text{M}$  NaI and 200  $\mu\text{L}$  of acetone (0.27 M in the growth solution) to the growth solution. The resulting electrodeposited particles are large THH with tip truncations (Fig. 10B).

The  $[\text{Pd}^{2+}]$ -dependent shape gradient developed for electrodeposition in BioUltra A CTAB was also replicated in dried BioUltra B CTAB using the same additive conditions. Growth solutions containing 0.30 mM and 0.061 mM  $\text{H}_2\text{PdCl}_4$  were modified with 0.68  $\mu\text{M}$  NaI and 200  $\mu\text{L}$  of acetone (0.27 M in growth solution), and a current of  $-2.04 \mu\text{A cm}^{-2}$  was applied for 3 hours. The products obtained were RD and CC, respectively (Fig. 10A and C). Both shaped samples do display some size dispersity and, like the BioUltra A electrodeposited CC sample, the low  $[\text{Pd}^{2+}]$  condition also produced some poorly-

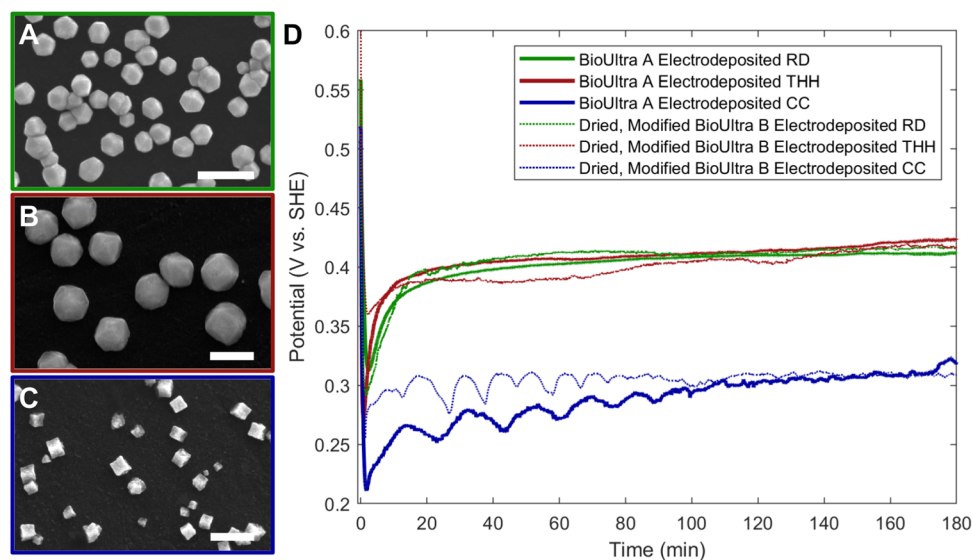


**Fig. 10** Electrodeposited Pd particles in dried BioUltra B CTAB with 0.68  $\mu\text{M}$  NaI and 200  $\mu\text{L}$  of acetone (0.27 M) added to the growth solution. All other conditions are identical to the electrochemical synthesis of Pd particles in BioUltra A CTAB. SEM images of (A) RD (0.30 mM  $\text{Pd}^{2+}$ ), (B) THH (0.12 mM  $\text{Pd}^{2+}$ ), (C) Electrodeposited CC (0.061 mM  $\text{Pd}^{2+}$ ), and (D) chronopotentiometry measurements of each electrodeposition synthesis, compared to chronopotentiometry measurements of identical syntheses in BioUltra A. Scale bars: 300 nm.



formed and multiply-twinned side products. The RD formed at the higher  $[Pd^{2+}]$  condition (0.30 mM  $Pd^{2+}$ ) are slightly smaller than the RD electrodeposited in BioUltra A. However, the morphological results are in significantly better agreement with the products of the BioUltra A electrodeposition synthesis (Fig. 5) than the electrodeposition attempts in as-received, unmodified BioUltra B (Fig. S8<sup>†</sup>). Comparison of chronopotentiometric data from the dried, modified BioUltra B electrodeposition synthesis also shows an improvement in agreement with the chronopotentiometry traces from the BioUltra A electrodeposition syntheses (Fig. 10D).

### Probing generalizability to other solvents

To determine whether acetone is unique in its ability to fine-tune nanoparticle growth in this synthesis, short-chain alcohols were tested as additives. Addition of 0.68  $\mu$ M NaI and 50  $\mu$ L of neat ethanol (0.086 M) or methanol (0.12 M) into a standard growth solution in as-received BioUltra B CTAB produces THH products, just as acetone does (Fig. S24B and S24C<sup>†</sup>). Interestingly, the shape evolution leading to THH formation appears somewhat insensitive to the type of solvent added; when 0.48  $\mu$ M NaI and 200  $\mu$ L of neat acetone (0.27 M), ethanol (0.34 M), or methanol (0.49 M) are added to a standard growth solution in as-received BioUltra B CTAB, all samples display THH-like morphology, with acetone and ethanol leading to similar-looking truncations and smaller side products (Fig. S24<sup>†</sup>). Adding isopropanol or ethanol at the same volumes (150  $\mu$ L to 300  $\mu$ L) as acetone into a dried BioUltra B growth solution with all conditions standard for THH production (along with 0.68  $\mu$ M NaI) led to well-formed THH and truncated THH, with optimal THH produced with 240  $\mu$ L of isopropanol (0.31 M) or 160 to 180  $\mu$ L of ethanol (0.27 M to 0.31 M) (Fig. 11A–C). Curiously, adding methanol at volumes ranging from 110  $\mu$ L to 240  $\mu$ L (0.27 M to 0.59 M), along with iodide, always leads to THH formation (Fig. 11D and E). Methanol is known to be less effective than ethanol or other longer-chain alcohols at partitioning into micelles and bilayers and generally needs to be present in solution at higher concentrations to have similar structure-modifying effects.<sup>32,37,38,41,43,44</sup> Methanol's lower efficacy at affecting CTAB behavior might in turn cause it to have different or less pronounced effects on Pd activity than other solvent additives,

creating a broader THH-stabilizing range of solvent addition. All solvents produce nanoparticles with low size dispersity within an individual sample of optimized THH, but there is some variation in the size of THH between solvents, which likely could be further mitigated by slightly adjusting the concentration of seed colloid solution added to the reaction.

The isopropanol and ethanol addition results, which are in good correspondence with what is seen from acetone addition, suggest that the individual chemical identity of the molecular contaminant does not specifically matter, but rather its disruption of the local concentration or arrangement of CTAB at the growing particles' surface, which may be related to steric bulk and/or polarity. The ability to stabilize THH with a range of different solvent additives also implies that subtle effects on solution viscosity (and, in turn, its effects on diffusion rate of the metal precursor and/or reducing agent) are not the cause of the contaminant-driven kinetic changes. Methanol's low viscosity is similar to that of acetone, while the two other alcohols tested are more viscous at room temperature, and yet the results of acetone addition are far more similar to the products generated by using isopropanol or ethanol than to results with methanol. A mechanism related to the diffusion rate or other mass transport limitations of the reducing agent is also not supported by the fact that both the effects of different CTAB formulations and of acetone addition can be seen in the product morphologies of electrodeposition syntheses, where the electron supply rate is held constant and no chemical reducing agent is present.

These results, in combination with the knowledge that methanol has lower efficacy than other solvents tested at disturbing micelle and bilayer structure, suggest that changes in CTAB bilayer structure due to the introduction of amphiphilic organic solvent impurities change the effective metal ion concentration near the nanoparticle surface, altering the measured solution potential and apparent growth kinetics. While we cannot rule out changes in the activity of  $Pd^{2+}$  ions in the broader reaction solution, there is a dominant surface-based influence of the impurity species since their influence is clearly seen in electrodeposition on a GCE surface. Some threshold concentration of solvent contamination is also necessary for this modification of the growth solution to be significant to shape control, as changes in particle mor-

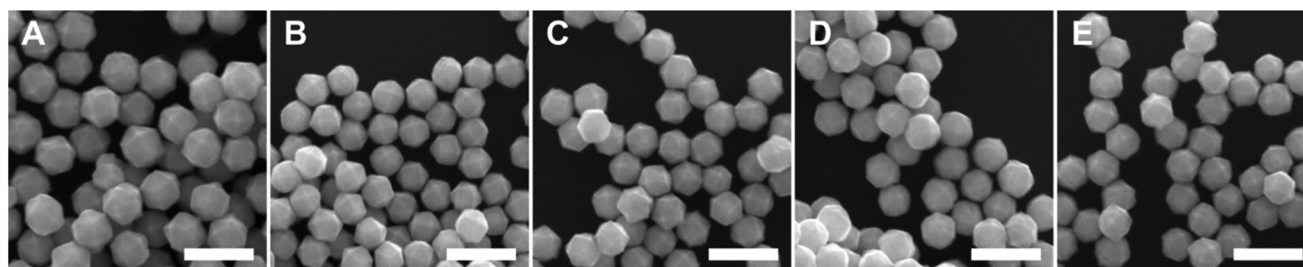


**Fig. 11** SEM images of Pd THH particles synthesized in dried BioUltra B CTAB with added NaI and different solvents. (A) 190  $\mu$ L of acetone (0.26 M), (B) 240  $\mu$ L of isopropanol (0.31 M), (C) 180  $\mu$ L of ethanol (0.31 M), (D) 110  $\mu$ L of methanol (0.27 M), (E) 240  $\mu$ L of methanol (0.59 M). All growth solution conditions standard, plus 0.68  $\mu$ M added NaI. Scale bars: 300 nm.



phology are not noted with  $0 < x < 0.16$  M acetone present (Fig. S14B†).

Related effects at the surface-solution interface are also hypothesized to be a possible mechanism of action for the shape-controlling role of iodide in this synthesis. By displacing a small number of surface-adsorbed bromide ions, low concentrations of iodide may disrupt the structure and stability of the CTAB bilayer on the nanoparticle surface, increasing permeability and diffusion in such a way that the local Pd ion concentration is effectively increased at the surface of a growing particle and/or the electrode surface. Changing the surface adsorption strength of CTAB by modifying CTA<sup>+</sup>-anion pairing interactions is expected to have a subtly different effect on particle growth kinetics compared to the effect of the intercalation of organic molecules into the bilayer at some small distance from the surface, which could explain why both additives are required for successful THH growth. Low micromolar concentrations of iodide, as in the present work, have also been shown to accelerate metal ion reduction for metals such as Pd, potentially by acting as a bridge between a metal ion and particle surface.<sup>12</sup>

## Conclusion

Line-to-line and lot-to-lot variations in commercial reagents, such as BioXtra vs. BioUltra A vs. BioUltra B CTAB, have significant synthetic consequences for the robust and reproducible synthesis of shape-controlled nanomaterials. We have identified multifactorial contamination from both elemental inorganic and molecular organic sources in multiple CTAB varieties as being responsible for differences in product morphology and we have used real-time electrochemical measurements to understand the influence of this contamination on the chemistry of the nanoparticle growth environment. Specifically, iodide (a known CTAB contaminant) and acetone (a previously unrecognized contaminant in powdered CTAB) are critical for establishing the precise local kinetic minimum required for successful formation of monometallic Pd THH. The sensitivity of this synthesis to reaction rate as modulated through the concentrations of Pd<sup>2+</sup> ions, NaI, and acetone, also provides a convenient way of synthesizing an array of other nanoparticle shapes such as concave cubes, terraced cubes, corner-truncated terraced cubes, and rhombic dodecahedra with only minor modifications to a single synthesis.

The identification of organic solvents as impurities in powdered commercial surfactants is likely to be of broader importance to the field of nanoparticle synthesis, as is the intentional use of organic solvent addition as a tool for reaction modification in aqueous syntheses of shaped metal nanoparticles. Though organic impurities are not as widely considered as inorganic contamination when troubleshooting particle synthesis in aqueous reactions, solvent contamination can change the reducing environment indirectly through modification of surfactant behavior, which in turn changes metal activity. In this case, the adventitious presence of

acetone facilitated the development of a synthesis for monometallic Pd THH. However, for nanoparticle syntheses where trace amounts of solvents are not required or where their role is unknown or unstudied, oven-drying as-received powdered commercial surfactants for precise control over solvent content may be best practice going forward. Solvent is not an obvious contaminant for dried, high-purity powders, although in retrospect the macroscopic crystalline structure of the different CTAB varieties does differ slightly, from diffuse powders to more crystalline samples. Possible solvent contamination in surfactants such as cetyltrimethylammonium chloride (CTAC)—which is sometimes received as a 25 wt% aqueous solution—may also merit further consideration and could be responsible for variations in products occasionally observed with different lots of this reagent for shaped gold (Au) and Pd nanoparticle syntheses (unpublished results).

More generally, we have shown that time-resolved electrochemical measurement is a useful methodology for monitoring reaction progress and that it has promise as a widely implementable method for benchmarking the solution potentials of newly developed and existing colloidal syntheses. Time-resolved measurement of solution potential is a contaminant-agnostic troubleshooting tool for redox reactions, as it is responsive to changes in solution potential due to both elemental and molecular impurities. This is particularly important when considering the possibility of alcohol impurities in aqueous growth solutions, as these cannot be easily identified *via* proton NMR, as well as acetone contamination at low levels which could be assumed to be a residue in an NMR tube from previous use. Real-time electrochemical measurements also provide information about possible mechanisms by which contaminants influence particle growth, something that is not as easily discerned from combinatorial synthesis and imaging approaches. Consequently, due to its flexibility, cost-effectiveness, and ease of implementation, benchmarking of nanoparticle syntheses using a solution potential measurement as they are developed could provide an avenue for easier troubleshooting of emerging reproducibility issues.

## Conflicts of interest

There are no conflicts of interest to declare.

## Acknowledgements

This material is based upon work supported by the National Science Foundation under Grant No. CHE-2406130. Acknowledgement is made to the donors of The American Chemical Society Petroleum Research Fund for partial support of this research (57708-DNI10). SEM and STEM imaging was conducted at the University of Virginia Nanoscale Materials Characterization Facility (NMCF) and additional SEM imaging was conducted at the Wesleyan University Advanced





Instrumentation Center. NMR spectroscopy was conducted at the University of Virginia Biomolecular Magnetic Resonance Facility, which is supported by the University of Virginia School of Medicine.

## References

- 1 J. De Roo, *Chem. Mater.*, 2022, **34**, 5766–5779.
- 2 E. N. Lang, C. J. Pintro and S. A. Claridge, *Chem. Mater.*, 2022, **34**, 5273–5282.
- 3 S. Jharimune, R. Pfukwa, Z. Chen, J. Anderson, B. Klumperman and R. M. Rioux, *J. Am. Chem. Soc.*, 2021, **143**, 184–195.
- 4 L. M. Liz-Marzán, C. R. Kagan and J. E. Millstone, *ACS Nano*, 2020, **14**, 6359–6361.
- 5 R. E. Abutbul and Y. Golan, *Nanotechnology*, 2020, **32**, 102001.
- 6 R. G. Rayavarapu, C. Ungureanu, P. Krystek, T. G. van Leeuwen and S. Manohar, *Langmuir*, 2010, **26**, 5050–5055.
- 7 D. K. Smith and B. A. Korgel, *Langmuir*, 2008, **24**, 644–649.
- 8 J. E. Millstone, W. Wei, M. R. Jones, H. Yoo and C. A. Mirkin, *Nano Lett.*, 2008, **8**, 2526–2529.
- 9 A. C. Alba-Rubio, P. Christopher, M. L. Personick and K. J. Stowers, *J. Catal.*, 2024, **429**, 115259.
- 10 E. N. Lang and S. A. Claridge, *Nanotechnology*, 2021, **33**, 082501.
- 11 L. Scarabelli, A. Sánchez-Iglesias, J. Pérez-Juste and L. M. Liz-Marzán, *J. Phys. Chem. Lett.*, 2015, **6**, 4270–4279.
- 12 M. E. King, I. A. Kent and M. L. Personick, *Nanoscale*, 2019, **11**, 15612–15621.
- 13 N. S. R. Satyavolu, A. S. Peinetti, Y. Wang, A. S. Ali, J. W. Lin and Y. Lu, *Chem. Mater.*, 2019, **31**, 2923–2929.
- 14 X. Ye, M. R. Jones, L. B. Frechette, Q. Chen, A. S. Powers, P. Ercius, G. Dunn, G. M. Rotskoff, S. C. Nguyen, V. P. Adiga, A. Zettl, E. Rabani, P. L. Geissler and A. P. Alivisatos, *Science*, 2016, **354**, 874–877.
- 15 Y.-Y. Li, H.-G. Liao, L. Rao, Y.-X. Jiang, R. Huang, B.-W. Zhang, C.-L. He, N. Tian and S.-G. Sun, *Electrochim. Acta*, 2014, **140**, 345–351.
- 16 T. Ming, W. Feng, Q. Tang, F. Wang, L. Sun, J. Wang and C. Yan, *J. Am. Chem. Soc.*, 2009, **131**, 16350–16351.
- 17 N. Tian, Z.-Y. Zhou, N.-F. Yu, L.-Y. Wang and S.-G. Sun, *J. Am. Chem. Soc.*, 2010, **132**, 7580–7581.
- 18 H. Lin, Z. Lei, Z. Jiang, C. Hou, D. Liu, M. Xu, Z. Tian and Z. Xie, *J. Am. Chem. Soc.*, 2013, **135**, 9311–9314.
- 19 S. P. McDarby, C. J. Wang, M. E. King and M. L. Personick, *J. Am. Chem. Soc.*, 2020, **142**, 21322–21335.
- 20 D. K. Smith, N. R. Miller and B. A. Korgel, *Langmuir*, 2009, **25**, 9518–9524.
- 21 S. Ghosh and L. Manna, *Chem. Rev.*, 2018, **118**, 7804–7864.
- 22 W. Du, S. Deng, S. Chen, S. Jin, Y. Zhen, Y. Pei and M. Zhu, *J. Phys. Chem. Lett.*, 2021, **12**, 6654–6660.
- 23 M. R. Langille, M. L. Personick, J. Zhang and C. A. Mirkin, *J. Am. Chem. Soc.*, 2012, **134**, 14542–14554.
- 24 O. M. Magnussen, *Chem. Rev.*, 2002, **102**, 679–726.
- 25 J. Lipkowski, Z. Shi, A. Chen, B. Pettinger and C. Bilger, *Electrochim. Acta*, 1998, **43**, 2875–2888.
- 26 Y. Xia, X. Xia and H.-C. Peng, *J. Am. Chem. Soc.*, 2015, **137**, 7947–7966.
- 27 H. H. Kim, S. W. Im, N. H. Cho, S. Choi, S. Kim, Y.-C. Lim and K. T. Nam, *J. Phys. Chem. Lett.*, 2022, **13**, 8344–8351.
- 28 N. R. Babij, E. O. McCusker, G. T. Whiteker, B. Canturk, N. Choy, L. C. Creemer, C. V. D. Amicis, N. M. Hewlett, P. L. Johnson, J. A. Knobelsdorf, F. Li, B. A. Lorschach, B. M. Nugent, S. J. Ryan, M. R. Smith and Q. Yang, *Org. Process Res. Dev.*, 2016, **20**, 661–667.
- 29 I. Bibi, S. W. H. Shah, M. Bibi, W. Rehman, L. A. Shah, O. ur R. Abid and W. Khan, *Asia-Pac. J. Chem. Eng.*, 2021, **16**, e2718.
- 30 M. Hossain and G. J. Blanchard, *Chem. Phys. Lipids*, 2021, **238**, 105091.
- 31 F. Golmohammadi, M. Amiri, H. Gharibi, A. Yousefi and M. Safari, *J. Solution Chem.*, 2020, **49**, 16–33.
- 32 M. H. L. Nguyen, M. DiPasquale, B. W. Rickeard, C. B. Stanley, E. G. Kelley and D. Marquardt, *Biophys. J.*, 2019, **116**, 755–759.
- 33 A. K. Sood, H. Kaur and T. S. Banipal, *Arabian J. Chem.*, 2019, **12**, 3847–3862.
- 34 H. Jiang, G. Beaucage, K. Vogtt and M. Weaver, *J. Colloid Interface Sci.*, 2018, **509**, 25–31.
- 35 I. Setiawan and G. J. Blanchard, *J. Phys. Chem. B*, 2014, **118**, 537–546.
- 36 Y. O. Posokhov and A. Kyrychenko, *Comput. Biol. Chem.*, 2013, **46**, 23–31.
- 37 T. Sidim and G. Acar, *J. Surfactants Deterg.*, 2013, **16**, 601–607.
- 38 H. I. Ingólfsson and O. S. Andersen, *Biophys. J.*, 2011, **101**, 847–855.
- 39 A. A. Gurtovenko and J. Anwar, *J. Phys. Chem. B*, 2009, **113**, 1983–1992.
- 40 Y. Wang and P. Dea, *J. Chem. Eng. Data*, 2009, **54**, 1447–1451.
- 41 M. Patra, E. Salonen, E. Terama, I. Vattulainen, R. Faller, B. W. Lee, J. Holopainen and M. Karttunen, *Biophys. J.*, 2006, **90**, 1121–1135.
- 42 W. Niu, L. Zhang and G. Xu, *ACS Nano*, 2010, **4**, 1987–1996.
- 43 M. Sonmez, H. Y. Ince, O. Yalcin, V. Ajdžanović, I. Spasojević, H. J. Meiselman and O. K. Baskurt, *PLoS One*, 2013, **8**, e76579.
- 44 N. Nishikido, Y. Moroi, H. Uehara and R. Matuura, *Bull. Chem. Soc. Jpn.*, 1974, **47**, 2634–2638.

